ELSEVIER

Journal of Alloys and Compounds 300–301 (2000) 316–321

Journal of ALLOYS AND COMPOUNDS

www.elsevier.com/locate/jallcom

ESR and X-ray diffraction measurements of Nd substituted yttrium aluminum garnet films

R. Jabłonski, J. Sarnecki*, K. Mazur, J. Sass, J. Skwarcz

Institute of Electronic Material Technology, 133 Wólczyńska Str., Warsaw 01-919, Poland

Abstract

Yttrium aluminum garnet (YAG) layers, doped with some rare-earth ions can be used as thin film solid-state lasers. Thin films of Nd^{3+}-doped YAG have been grown on undoped YAG substrates by the isothermal liquid phase epitaxy (LPE) dipping technique. The layers have been obtained from a supercooled molten garnet-flux high temperature solution. $Y_{3-x}Nd_xAl_5O_{12}$ films (2–30 μm) grown on the (111) plane of YAG substrate have been investigated as a function of neodymium concentration using electron spin resonance (ESR) and X-ray diffraction techniques. According to those measurements it can be concluded that the obtained thin films possess high quality.
© 2000 Elsevier Science S.A. All rights reserved.

Keywords: ESR; YAG substrates; Neodymium; X-ray diffraction

1. Introduction

Rare earth doped yttrium aluminum garnet (YAG) epitaxial layers possess excellent lasing properties. The first epitaxial Ho^{3+} and Nd^{3+} doped YAG laser layers on pure YAG substrates were reported by Van der Ziel et al. in 1972 [1]. During the last few years much attention has been focused on IR diode lasers – pumping solid state lasers with planar monocrystalline structures. These devices allow fabrication of planar active components for fiberoptic communication. The most promising material for this purpose is rare earth doped yttrium aluminum garnet ($Y_3Al_5O_{12}$).

Planar active optical structures in garnet crystals are fabricated by two basic techniques: ion implantation and epitaxy. Ion implantation has been the principal technique for fabrication of planar active optical structures within laser-gain media such as Er:YAG, Nd:YAG or Nd:GGG [2–4]. Liquid phase epitaxy (LPE) has been employed for growing rare earth doped YAG and GGG laser waveguiding layers on the YAG and GGG substrates [5–7]. Liquid phase epitaxy is a technique suitable for production of epitaxial thin film lasers with a quality higher than that of the implanted structures [8]. In this study, the lattice distortions in grown YAG/YAG:Nd^{3+} films were investigated by the ESR and X-ray diffraction techniques.

2. Experimental

2.1. LPE growth of Nd:YAG films

For growing of Nd:YAG thin garnet layers the method of liquid phase epitaxy (LPE) was chosen. We applied the LPE technique that has been used in several laboratories for iron-garnet epitaxy in the case of the nonmagnetic garnets YAG and GGG.

The layers were grown from a supercooled (supersaturated) molten garnet-flux high temperature solution. Standard isothermal LPE dipping technique with reversed axial rotation has been used to obtain YAG thin films doped with Nd^{3+} ions. The ΔT which is the difference between the saturation temperature T_S and the growth temperature T_G is necessary to obtain the epitaxial growth of garnet layer from the garnet-flux ($PbO–B_2O_3$) solution.

The composition of molten garnet–$PbO–B_2O_3$ high temperature solution is specified by the following parameters:

$$R_1 = \frac{[Al_2O_3]}{[Y_2O_3 + Nd_2O_3]}, R_3 = \frac{[PbO]}{[B_2O_3]}, R_5 = \frac{[Y_2O_3]}{[Nd_2O_3]}$$

and

$$R_4 = \frac{[Y_2O_3 + Al_2O_3 + Nd_2O_3]}{[Y_2O_3 + Al_2O_3 + Nd_2O_3 + PbO + B_2O_3]}.$$

The same molar ratios of the melted compounds were used by Blank et al. for the epitaxy of magnetic garnets

*Corresponding author.
E-mail address: palma@sp.itme.edu.pl (J. Sarnecki)

0925-8388/00/$ – see front matter © 2000 Elsevier Science S.A. All rights reserved.
PII: S0925-8388(99)00731-8

Table 1
R_i parameters

No.	R_1	R_3	R_4	R_5	T_G (°C)	ΔT (°C)	f_G (μm/min)	$\Delta\theta_{444}$ (arcsec)	$\Delta a/a_S \times 10^4$	x	at.%
4	5.0	12.0	0.0275	14.0	970	20	1.0	0	0	~0.03	1
7	4.1	12.0	0.0284	3.5	989	15	0.4	−48.9	4.8	0.088	2.9
13	3.4	12.0	0.0295	1.75	1003	12	0.5	−105.1	10.2	0.186	6.2

[9]. The R_i parameters are important in controlling the growth conditions and properties of the films. The R_i parameters are listed in Table 1 for the Nd:YAG films grown with different values of: neodymium concentrations, growth temperatures, supersaturations (ΔT), growth rates f_G, fractional mismatches $\Delta a/a_S = (a_F - a_S)/a_S$ (where a_F and a_S are film and substrate lattice constants, respectively), estimated from $\Delta a/a$ measurements, compositional parameters x (in the formula $Y_{3-x}Nd_xAl_5O_{12}$) and the concentrations of Nd^{3+} ions in the films.

Epitaxial Nd:YAG layers were grown on both sides of the polished (111) YAG substrates. The substrate off-orientation was about 4°.

2.2. The measurements

The samples of (typical) size 3.5×3.5 mm were cut from the epitaxial structure Nd^{3+}:YAG/YAG. The ESR spectra were measured with a Bruker ESP-300 spectrometer (X-band), equipped with a helium flow cryostat type ESR-900 from Oxford Instruments. The ESR lines were observed in the temperature range from 4 to 20 K.

Diffraction measurements were performed using X-ray quasi parallel double-crystal arrangement with 400 reflection on a Ge monochromator and 444 YAG reflection of Cu $K\alpha_1$ radiation. This arrangement allows one to obtain a well monochromatized and collimated high intensity primary beam with the wavelength dispersion $\Delta\lambda/\lambda \approx 2.8 \times 10^{-4}$, where $\Delta\lambda = 3.8 \times 10^{-3}$ Å is the difference between $K\alpha_1$ and $K\alpha_2$ spectral lines for Cu Kα radiation.

3. Results and discussion

3.1. ESR measurement

The width of paramagnetic lines (obtained in the temperature range 5 to 15) might be influenced by interaction of paramagnetic ions with surrounding nuclei, most probably related to the spatial distribution of the g factor caused by the lattice strains.

Other factors, such as T_1-spin–lattice interaction, T_2-spin–spin interaction have been assumed to be negligible in the first approximation. Resonance magnetic field H, for a paramagnetic ion is given by

$$H = \nu/(g\beta/h) - H_d \quad (1)$$

where ν is the microwave frequency, β is the Bohr magneton, h is Planck's constant, H_d is the local magnetic field produced by the surrounding nuclear dipoles, $g^2 = g_x^2 l^2 + g_y^2 m^2 + g_z^2 n^2$, l, m, n are direction cosines for plane (111),

$$g = [1/3 \sin^2\varphi\,(g_x^2 + 2g_z^2) + g_y^2 \cos^2\varphi]^{1/2}. \quad (2)$$

Values g and φ in Eq. (2) should be treated as averages for all ions. Each ion is characterized by $g_x + \delta g_x$, $g_y + \delta g_y$, $g_z + \delta g_z$, $\varphi + \delta\varphi$, δH_d, therefore, its resonant field differs from (1) by a value

$$\delta H = \delta H_d + \vartheta H/\vartheta g_x\,\delta g_x + \vartheta H/\vartheta g_y\,\delta g_y + \vartheta H/\vartheta g_z\,\delta g_z + \vartheta H/\vartheta\varphi\,\delta\varphi.$$

We have assumed that each of these five parameters varies independently of the others. As a result, the root mean square width of the ESR line is equal to (see Refs. [11–13]):

$$\langle\delta H^2\rangle = \left(\frac{\partial H}{\partial g_x}\right)^2\langle\delta g_x^2\rangle + \left(\frac{\partial H}{\partial g_y}\right)^2\langle\delta g_y^2\rangle + \left(\frac{\partial H}{\partial g_z}\right)^2\langle\delta g_z^2\rangle + \left(\frac{\partial H}{\partial\varphi}\right)^2\langle\delta\varphi^2\rangle + \left(\frac{\partial H}{\partial H_d}\right)^2\langle\delta H_d\rangle =$$

$$\langle\delta H_d^2\rangle + (h\nu/g^3\beta)^2\{1/9\; g_x^2 \sin^4\varphi\,\langle\delta g_x^2\rangle + g_y^2\cos^4\varphi\,\langle\delta g_y^2\rangle +$$

$$4/9 g_z^2 \sin^4\varphi\,\langle\delta g_z^2\rangle +$$

$$+ 1/4 \sin^2 2\varphi[1/3(g_x^2 + 2g_z^2) - g_y^2]^2\,\langle\delta\varphi^2\rangle. \quad (3)$$

By neglecting $\langle\delta g_x^2\rangle$, $\langle\delta g_y^2\rangle$, $\langle\delta g_z^2\rangle$ with respect to $\langle\delta\varphi^2\rangle$ one obtains:

$$\langle\delta H^2\rangle = \langle\delta H_d^2\rangle + (h\nu/g^3\beta)^2\; 1/4 \sin^2 2\varphi[1/3(g_x^2 + 2g_z^2) - g_y^2]^2\,\langle\delta\varphi^2\rangle. \quad (4)$$

The observed linewidth ΔH_{pp} will be related to δH by a constant K (for Gaussian line shape $K = 4$)

$$\Delta H_{pp}^2 = K\langle\delta H^2\rangle. \quad (5)$$

For example in Fig. 1a angular dependence for sample no. 4 for the (111) plane is shown. We observe an anisotropic spectrum of six magnetically inequivalent complexes with the effective spin $S = 1/2$ and $I = 0$ [13,14]. A difference between experimental points and

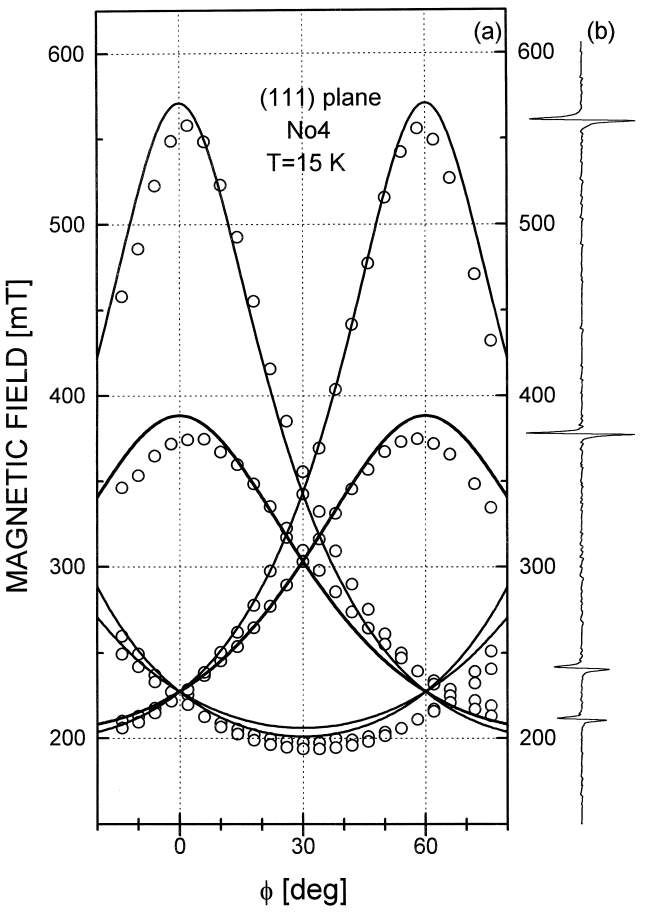

Fig. 1. (a) The angular dependence of the X-band ESR lines at 15 K of Nd^{3+}:YAG films with magnetic field in the (111) plane; circles are experimental data, solid lines are theoretical curves obtained with $g_x = 1.733$, $g_y = 1.179$, $g_z = 3.915$. (b) ESR spectrum for $H \| [110]$ ($\varphi = 0$).

theoretical solid lines with $g_x = 1.739$, $g_y = 1.179$ and $g_z = 3.915$ results from the 4–5° disorientation. Additionally, in Fig. 1b the ESR spectrum for magnetic field $H \| [110]$ ($\varphi = 0$) is presented.

Fig. 2a shows temperature dependence of the ESR amplitude for microwave power $P = 2$ mW. The signal intensity decreases as $1/T$ for the samples no. 7 and no. 13. For the sample no. 4 at temperatures higher than 'a' the saturation effect is negligible and similar to samples no. 7 and no. 13.

According to Fig. 2b, temperature ~15 K has been chosen for the performance dependencies of the ESR amplitudes and linewidths. They are depicted vs. power in Fig. 2c and d. With the use of the above mentioned dependencies the T_1 and T_2 parameters have been obtained. The results are shown in Table 2. The results of the measurement shown in Fig. 2 have been attained for the complex no. 5 (see Fig. 1) with the principal axes:

$x - [1\bar{1}0]$, $y - [110]$, $z - [001]$.

In Fig. 3a the experimental data of angular dependence linewidth and theoretical curves for the sample nos. 4, 7, and 13 are presented. The fitting was performed with the use of Eqs. (4) and (5) for $-20° < \varphi < +30°$. Results are presented in Table 2 and shown in Fig. 4.

3.2. X-ray diffraction measurements

The lattice spacings were measured by X-ray high resolution diffraction. The present measurements were performed step by step with the constant counting time (5 s). Fig. 3b shows the XRD patterns of the Nd:YAG films grown on YAG substrates under conditions which are given in Table 1. The changes of Bragg angle difference $\Delta\theta_{444} = \theta_F - \theta_S$ are due to the difference in the lattice spacing between epitaxial film and substrate and are also listed in Table 1.

The recorded rocking curve, shown in the Fig. 3b, exhibited two maxima corresponding, respectively, to the reflections from the epitaxial layer and the substrate.

From the measured angular spacing between the two peaks one can calculate the difference between the interplanar spacing at the substrate and the epitaxial layer. The substitution of yttrium by neodymium in dodecahedral sites leads to the increase of the lattice mismatch. The garnet epitaxial films were compressed and presented elastic accommodation for the substrates. No cracks appeared in the thin garnet layers.

From the substrate layer misfit (fractional mismatch) the concentration of Nd^{3+} ions in strained Nd:YAG films was estimated using an empirical formula given by Strocka et al. [10]. The epitaxial films were doped with neodymium concentration up to about 6 at.%. The point to be noted is that growing of the Nd:YAG single crystals having lasing parameters with neodymium concentration higher then ~1.3 at.% is almost impossible.

In the case of specimen 4 the respective X-ray rocking curve indicates no peak separation. It means that the lattice constants of the film and the substrate are equal. This observation is obvious since the unsubstituted YAG layer obtained by the LPE method on a substrate which was cut from a YAG single crystal bowl has $a_F < a_S$. Thus the introduction of the neodymium of concentration about 1 at.% into the YAG film results in equality of the film and the substrate lattice constant [2].

4. Conclusions

The neodymium concentration in Nd^{3+}:YAG epitaxial layers was calculated from the ESR and X-ray diffraction measurements. The good agreement between obtained results has been obtained within about 15%. The relationship $\Delta H_{pp} = f(\langle\delta\varphi^2\rangle, \langle\delta H_d^2\rangle)$ at temperature ~15 K shows that there is an influence of the dopant concentration on the lattice deformation near the Nd^{3+} ion sites. This deformation depended on the $\langle\delta H_d^2\rangle$ parameter which increases

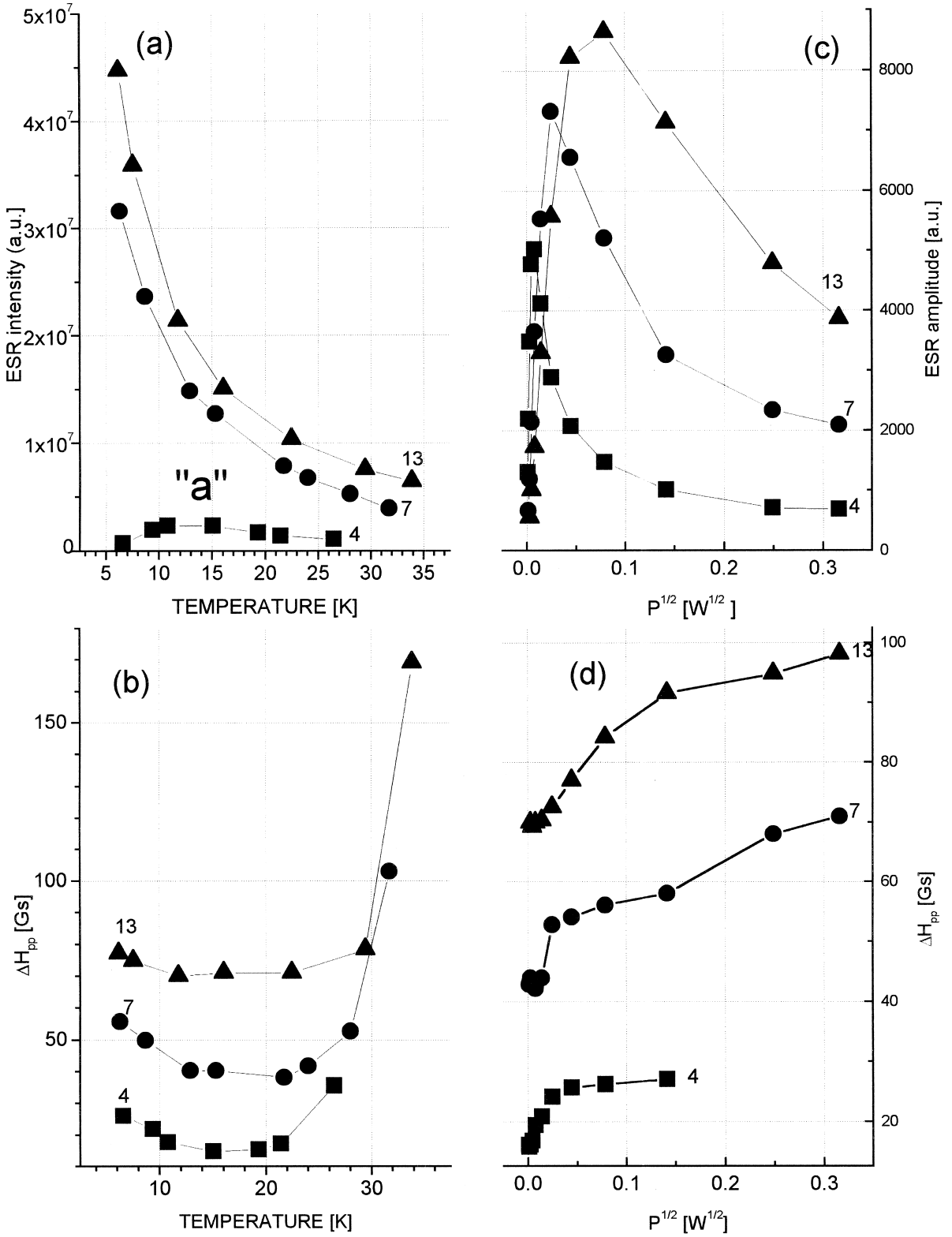

Fig. 2. The dependencies of ESR intensity (a) and linewidth (b) on temperature. The dependencies of ESR intensity (c) and linewidth (d) versus $P^{1/2}$, respectively.

with the Nd^{3+} concentration. The parameter $\langle \delta\varphi^2 \rangle$ also increases with the neodymium concentration. The minimal broadening of the ESR linewidth for the principal crystallographic directions has been observed. Such dependence is typical for mosaic structures. These parameters suggest local distortion caused by the lattice mismatch strains.

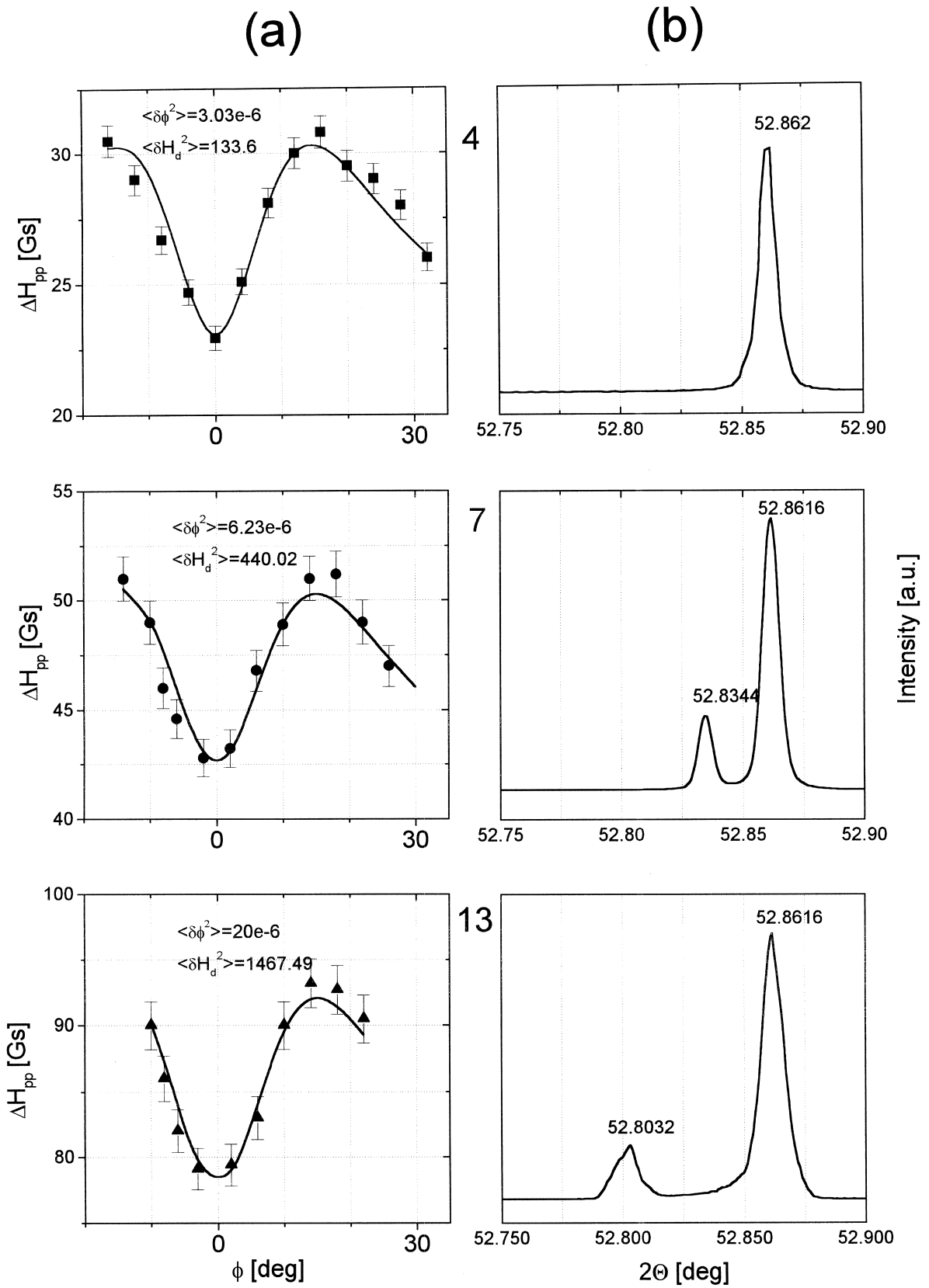

Fig. 3. (a) Data and fitted (Eqs. (4) and (5)) theoretical curves for the ESR linewidth. (b) Double crystal rocking curves for samples 4, 7 and 13, respectively (Cu Kα radiation).

Table 2
Results for samples no. 4, 7 and 13

No.	T_1 10^{-4} s	T_2 10^{-10} s	ΔH_{pp} Gs	$\langle \delta\varphi^2 \rangle$	$\langle \delta H_d^2 \rangle$ Gs	Relative intensity
4	51	6.3	23	3.0297e−6	133.06	1
7	9.13	2.52	43	6.2340e−6	440.02	3.0857
13	3.07	1.6	78	20.000e−6	1467.79	5.8368

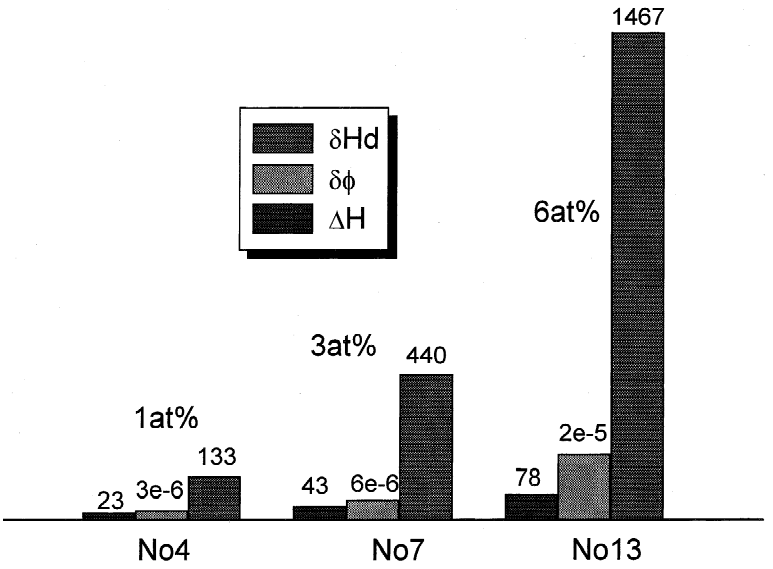

Fig. 4. The bar graph of $\langle \delta H_d^2 \rangle$, $\langle \delta\varphi^2 \rangle$, ΔH_{pp} for samples 4, 7 and 13, respectively.

They correspond to the angular difference $\Delta\theta_{444}$. Moreover, large decrease of the spin lattice time T_1 with increasing neodymium concentration demonstrates creation of the strains in the films.

References

[1] P. Van der Ziel, W.A. Bonner, L. Kopf, L.G. Van Uitert, Coherent emission from Ho^{3+} ions in epitaxially grown thin aluminum garnet films, Phys. Lett. 22 (1972) 105–106.
[2] L. Zhang, P.D. Towsend, P.J. Chandler, A.J. Silversmith, Upconversion in ion implanted Er:YAG waveguide, Elect. Lett. 30 (1994) 1063–1064.
[3] S.J. Field, D.C. Hanna, A.C. Large, D.P. Shepherd, A.C. Tropper, P.J. Chandler, P.D. Towsend, L. Zhang, Low threshold ion-implanted Nd:YAG waveguide laser, Elect. Lett. 25 (1989) 2375–2376.
[4] D.C. Hanna, J.K. Jones, A.C. Large, D.P. Shepherd, A.C. Tropper, P.J. Chandler, M.J. Rodman, P.D. Towsend, L. Zhang, Quasi-three level 1.03 μm laser operation of a planar ion-implanted Yb:YAG waveguide, Optics Omm. 99 (1993) 211–215.
[5] B. Ferrand, D. Pelenc, I. Charter, Ch. Wyon, Growth of LPE Nd:YAG single crystal layers, J. Cryst. Growth 128 (1993) 966–969.
[6] N. Sugimoto, Y. Chishi, Y. Katoh, M. Shimokozo, S. Sudo, A ytterbium- and neodymium-co-doped yttrium aluminium garnet-buried channel waveguide laser pumped at 0.81 μm, Appl. Phys. Lett. 67 (1995) 582–584.
[7] M. Shimokozo, N. Sugimoto, A. Tate, Y. Katoh, Room temperature operation of an Yb-doped $Gd_3Ga_5O_{12}$ buried channel waveguide laser at 1.025 μm wavelength, Appl. Phys. Lett. 68 (1996) 2177–2179.
[8] M. Malinowski, R. Piramidowicz, J. Sarnecki, W. Woliński, Infrared-to-blue-wavelength upconversion in GGG:Pr^{3+} thin film grown by liquid phase epitaxy, J. Phys. Condens. Matter 10 (1998) 1909–1916.
[9] S.L. Blank, J.W. Nielsen, The growth of magnetic garnet by liquid phase epitaxy, J. Cryst. Growth 17 (1972) 302–311.
[10] B. Strocka, P. Holst, W. Tolksdorf, An empirical formula for the calculation of lattice constants of oxide garnets based on substituted yttrium- and gadolinium-iron garnets, Philips J. Res. 33 (1978) 186–202.
[11] P.L. Scott, H.J. Stapleton, C. Wainstein, Paramagnetic resonance linewidths in some rare-earth double nitrates, Phys. Rev. 137 (1A) (1965) A71–A74.
[12] R.H. Dieck, in: Measurement Uncertainty Method and Applications, Instrument Society of America, 1997, p. 92.
[13] A. Abragam, B. Bleaney, in: Electron Paramagnetic Resonance of Transition Ions, Clarendon Press, Oxford, 1970, p. 206.
[14] R. Wolfe, M.D. Sturge, F.R. Merritt, L.G. Van Uitert, Facet-related site selectivity for rare-earth ions in yttrium aluminum garnet, Phys. Rev. Lett. 26 (25) (1971) 1570.